Supplementary Material

Indirect urea electro-oxidation by nickel(III) in alkaline medium: from kinetic and mechanism to reactor modeling

Guillaume Hopsort[a,*], Laure Latapie[a], Karine Groenen Serrano[a], Karine Loubière[a], Theodore Tzedakis[a,*]

[a] Laboratoire de Génie Chimique, Université de Toulouse, CNRS, INPT, UPS, Toulouse, France

*Corresponding authors:
Pr. Theodore Tzedakis, theodore.tzedakis@univ-tlse3.fr
Ph.D. applicant Guillaume Hopsort, guillaume.hopsort@univ-tlse3.fr

Index

Section SM. 1: Material

All the information concerning chemicals and solutions used in this work is summarized in the Table SM1 following:

Table SM1 Indexation of all chemicals and solutions used in this work

CAS n°	Name	Formula	Molecular weight ($g.mol^{-1}$)	Purity	Supplier	Batch n°
7681-52-9	Sodium hypochlorite	Na^+ OCl^-	74.44	14% Cl_2	VWR Chemicals	21H234009
1310-73-2	Sodium hydroxide	NaOH	40.00	97%	Fisher Scientific	2181225
57-13-6	Urea	CON_2H_4	60.05	>99.5%	Sigma-Aldrich	SLCB9837
1310-58-3	Potassium hydroxide	KOH	56.11	85%	Alfa Aesar	10225535
7789-12-0	Sodium dichromate dihydrate	$Na_2Cr_2O_7 \cdot 2H_2O$	298.00	>99%	Aldrich	58692-065
7783-85-9	Ammonium iron(II) sulfate hexahydrate (Mohr's salt)	$(NH_4)_2Fe(SO_4)_2 \cdot 6H_2O$	392.14	99%	Sigma-Aldrich	MKBV6451V
7647-01-0	Hydrochloric acid	HCl	36.46	*wt.*37%	Fisher Scientific	2171489
75-75-2	Methanesulfonic acid	CH_4O_3S	96.10	99%	Acros Organics	A0419723
Standard for pH						
	Buffer solution pH 7.01				Hanna instruments	3701
	Buffer solution pH 10 (borate)				Fisher Scientific	2187023
	Buffer solution pH 11.00 (boric acid, sodium hydroxide solution/potassium chloride)				Honeywell	L1610
	Buffer solution pH 12.00				Alfa Aesar	R25H066
	Buffer pH 13.00				Reagecon	32520K1
Standard for Ion Chromatography						
7632-00-0	Nitrite in aqueous solution	Na^+ NO_2^-	69.00	996 ± 8 $\mu g.mL^{-1}$	SCP Science	S2009A5024
12125-02-9	Ammonium in aqueous solution	NH_4^+ Cl^-	53.49	1006 ± 7 $\mu g.mL^{-1}$	SCP Science	S200407013
590-28-3	Potassium cyanate	KOCN	81.12	97%	Alfa Aesar	M08F008

At the beginning of the present work, a commercial nickel(III) powder was looked for. A supplier named American Elements provided a green powder with the following designation "99%+ Nickel Oxyhydroxide Nanopowder" (product code : NI-OOH-02-NP / CAS n°55070-72-9). As a reminder, nickel(II) has a light green color. To dispel any doubts about this powder, experiments were carried out by bringing into contact a urea solution with this powder. No chemical reaction could be demonstrated (no decrease of NPOC, no formation of the previously identified by-products), thus suggesting that this powder was made of nickel(II). Several characterization tests were done and confirmed this. Thus, all the results obtained in this article were performed by using this powder. As a precaution, a nickel(II) hydroxide powder from Thermo Scientific (CAS n° 12054-748-7 / Batch n°A0422008 / Molecular weight 92.70 $g.mol^-$

[1]) was purchased. As shown in Figure SM1, where both powders were compared by XDR analysis, they presented the same crystallographic structure.

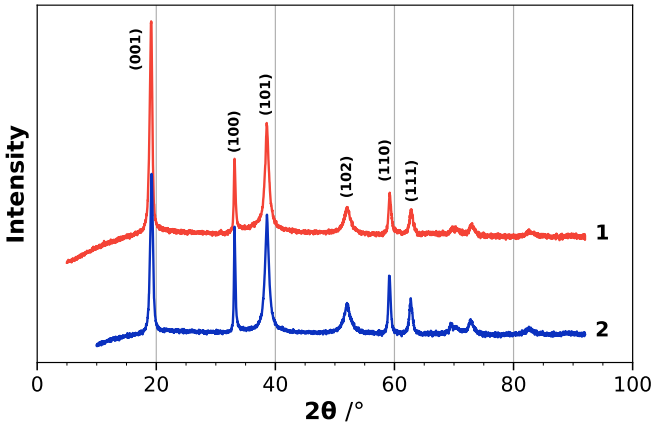

Figure SM1 XRD patterns of the nickel(II) powders purchased from (1) American Elements and (2) Thermo Scientific.

Section SM.2: Physical characterization of NiOOH

- *Set-up used for purity determination of synthesized nickel(III) powder*

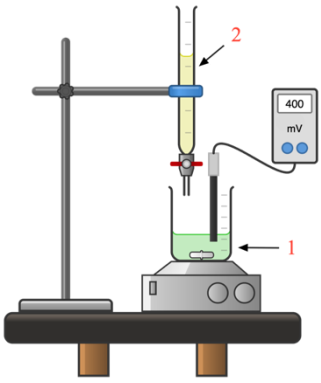

Figure SM2 Schematic representation of the experimental set-up used for determining the purity of the synthesized nickel(III) powder. Label 1 represents the nickel(III) particles dissolved in an acidic oxidized iron(III) solution at 7.20×10^{-2} mol.L^{-1} and label 2 represents the $K_2Cr_2O_7$ solution at 3.75×10^{-2} mol.L^{-1}.

Figure SM2 describes the experimental set-up used to evaluate the purity of nickel(III) in the synthesized powder. A precise amount of powder (137 mg) was mixed in a beaker filled with a solution composed of 30 mL of deionized water and 2 mL of hydrochloric acid. 882 mg of Mohr's salt was added, corresponding to a large excess of ferrous ions. A stirring period of 5 min was applied to obtain a total oxidation reaction between ferrous ions and nickel(III) particles. The last step consisted in determining the remaining ferrous ions (*i.e.*, the ones that

did not react) by a potentiometric titration with dichromate(VI) potassium. The equivalent volume was deduced from the rise in potential measured by a combined Pt ring electrode Metrohm®. An example of a potential *vs.* poured volume is shown in Figure SM3:

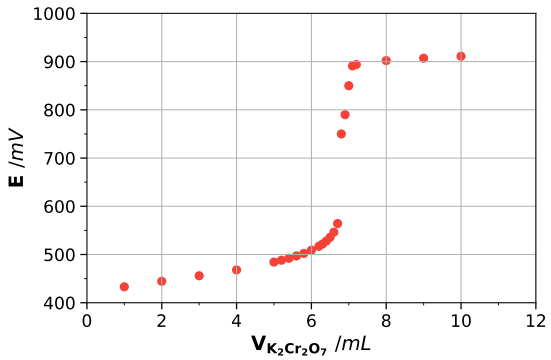

Figure SM3 Potentiometric titration curve involving 32 mL of a solution of nickel(III) particles dissolved in acidic oxidized iron(III) at 7.20×10^{-2} mol.L^{-1}, and a solution $K_2Cr_2O_7$ at 3.75×10^{-2} mol.L^{-1}.

At last, the amount of nickel(III) was equal to the amount of ferrous ions that reacted according to Eq. (SM. 1).

$$n_{Ni(III)} = n_{Fe(II)}^{\text{in excess}} - n_{Fe(II)}^{\text{titration}} \quad \text{(SM. 1)}$$

- *XRD analysis results*

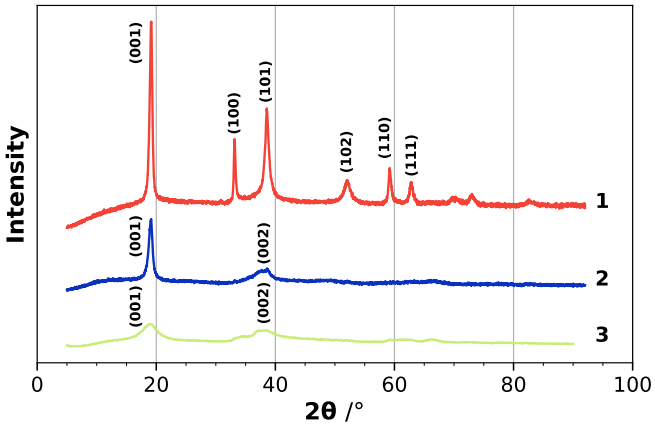

Figure SM4 XRD patterns of (1) commercial $Ni(OH)_2$ powder, (2) and (3) powders obtained by $Ni(OH)_2$ oxidation using respectively 0.176 and 0.768 mol.L^{-1} hypochlorite solutions (see §2.1.1).

- *SEM analysis results*

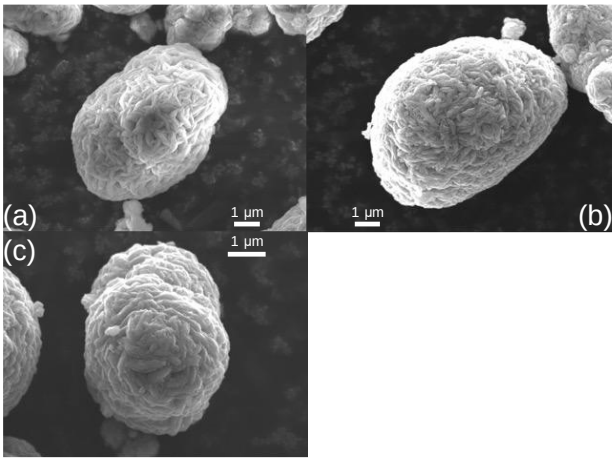

Figure SM5 SEM images of the samples (a) $Ni(OH)_2$ commercial powder (b) nickel(III) powder – sample 1 (c) nickel(III) powder – sample 2.

Section SM.3: Monitoring of the catalytic oxidation between urea and synthesized nickel(III) particle powder in alkaline medium

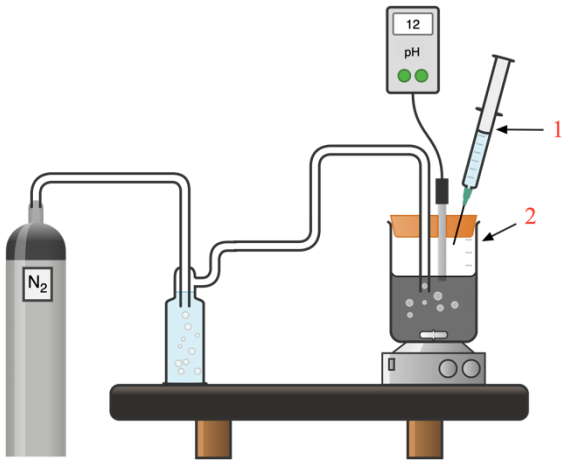

Figure SM6 Schematic representation of the experimental set-up used for studying the kinetics of the catalytic oxidation between urea and nickel(III) particles. Label 1 represents urea in a KOH solution and label 2 represents NiOOH particles in KOH solution in a thermoregulated cell under N_2 atmosphere.

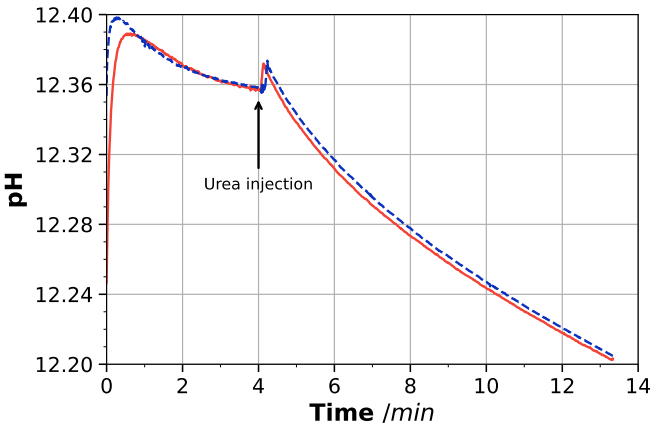

Figure SM7 Typical temporal variations of the pH when an alkaline urea solution was brought into contact with chemically synthesized nickel(III) sites. The repeatability of the results is represented here with two trials (solid and dashed lines).

Section SM.4: Repeatability of the measurements of the initial rate, r_χ^0, as a function of time chosen to calculate the initial rate from the curve $pH_{(t)}$

To ensure reliable and accurate measurements, the influence of the sampling time on the initial rate was studied. Table SM2 reports the different measures of the initial rate, noted r_χ^0, obtained for five reactant (urea and OH^-) concentrations and sampling times varying from 5 to 50 seconds. The relative standard deviation (RSD) was calculated from each averaged value of r_χ^0. This criterion allows identifying which sampling time was the best choice for determining r_χ^0.

Table SM2 Influence of the sampling on the repeatability of the initial reaction rate r_χ^0

Sampling time (s)		Experiment 1		Experiment 2		Experiment 3		Experiment 4		Experiment 5	
		Trial 1	*Trial 2*	*Trial 1*	*Trial 2*	*Trial 1*	*Trial 2*	*Trial 1*	*Trial 2*	*Trial 1*	*Trial 2*
5	r_χ^0 (mol.L^{-1}.s^{-1})	1.23×10^{-5}	1.40×10^{-5}	1.57×10^{-5}	1.64×10^{-5}	2.11×10^{-5}	1.67×10^{-5}	2.32×10^{-5}	1.98×10^{-5}	2.01×10^{-5}	2.01×10^{-5}
	Average	1.31×10^{-5}		1.61×10^{-5}		1.89×10^{-5}		2.15×10^{-5}		2.01×10^{-5}	
	Standard deviation (SD, mol.L^{-1}.s^{-1})	1.18×10^{-6}		4.97×10^{-7}		3.12×10^{-6}		2.39×10^{-6}		4.11×10^{-8}	
	Relative standard deviation (RSD)	9%		3%		17%		11%		0%	
10	r_χ^0 (mol.L^{-1}.s^{-1})	1.22×10^{-5}	1.38×10^{-5}	1.55×10^{-5}	1.62×10^{-5}	2.08×10^{-5}	1.66×10^{-5}	2.29×10^{-5}	1.96×10^{-5}	2.01×10^{-5}	2.03×10^{-5}
	Average	1.30×10^{-5}		1.59×10^{-5}		1.87×10^{-5}		2.13×10^{-5}		2.02×10^{-5}	
	SD (mol.L^{-1}.s^{-1})	1.15×10^{-6}		5.02×10^{-7}		3.03×10^{-6}		2.32×10^{-6}		1.84×10^{-7}	
	RSD	9%		3%		16%		11%		1%	
25	r_χ^0 (mol.L^{-1}.s^{-1})	1.18×10^{-5}	1.33×10^{-5}	1.50×10^{-5}	1.57×10^{-5}	2.01×10^{-5}	1.62×10^{-5}	2.22×10^{-5}	1.92×10^{-5}	2.00×10^{-5}	2.11×10^{-5}
	Average	1.25×10^{-5}		1.54×10^{-5}		1.81×10^{-5}		2.07×10^{-5}		2.05×10^{-5}	
	SD (mol.L^{-1}.s^{-1})	1.08×10^{-6}		4.65×10^{-7}		2.76×10^{-6}		2.11×10^{-6}		8.40×10^{-7}	
	RSD	9%		3%		15%		10%		4%	
50	r_χ^0 (mol.L^{-1}.s^{-1})	1.12×10^{-5}	1.25×10^{-5}	1.43×10^{-5}	1.50×10^{-5}	1.89×10^{-5}	1.56×10^{-5}	2.12×10^{-5}	1.86×10^{-5}	1.97×10^{-5}	2.24×10^{-5}
	Average	1.18×10^{-5}		1.46×10^{-5}		1.73×10^{-5}		1.99×10^{-5}		2.11×10^{-5}	
	SD (mol.L^{-1}.s^{-1})	9.67×10^{-7}		4.74×10^{-7}		2.35×10^{-6}		1.82×10^{-6}		1.87×10^{-6}	
	RSD	8%		3%		14%		9%		9%	
	Average global	1.26×10^{-5}		1.55×10^{-5}		1.83×10^{-5}		2.08×10^{-5}		2.05×10^{-5}	
	SD global (mol.L^{-1}.s^{-1})	5.70×10^{-7}		6.43×10^{-7}		7.39×10^{-7}		7.14×10^{-7}		4.32×10^{-7}	
	RSD global	5%		4%		4%		3%		2%	

From these findings, a sampling time of 10 seconds was chosen for calculating all the initial reaction rates.

Section SM.5: Variations of the kinetic constant k_χ for a sampling of 35 trials

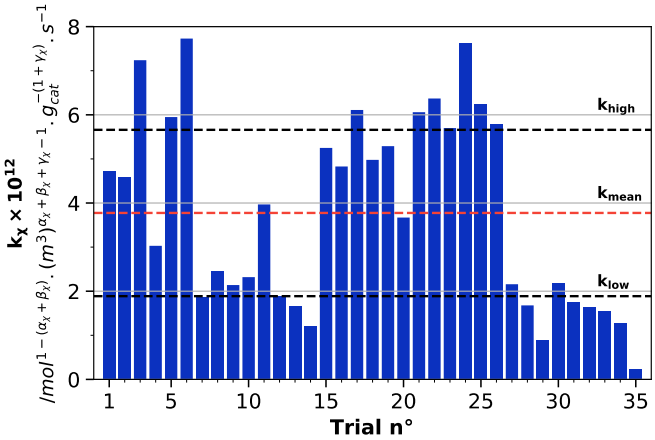

Figure SM8 Distribution histogram of the determined kinetic constant k_χ for the 35 experiments carried out. The values were ranged between 2.4×10^{-13} and 7.7×10^{-12} with a mean value at 3.8×10^{-12} $mol^{0.2}.(m^3)^{1.7}.g_{cat}^{-2.9}.s^{-1}$.

Section SM.6: Variations of the kinetic constant $k_{E\chi}$ for a sampling of 11 trials

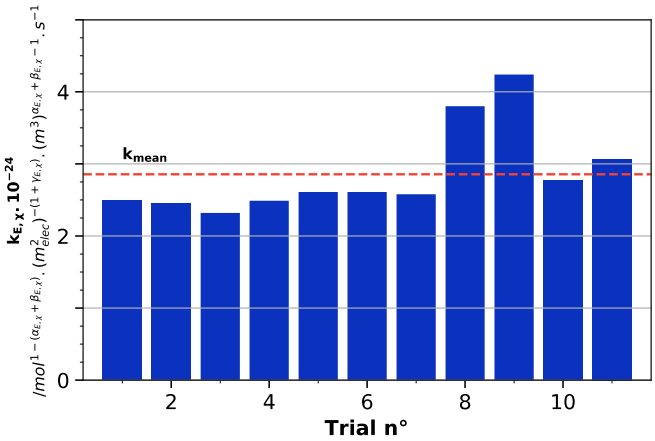

Figure SM9 Distribution histogram of the determined kinetic constant $k_{E\chi}$ for the 11 experiments carried out. The values were ranged between 2.32×10^{24} and 4.24×10^{24} with a mean value at 2.86×10^{24} $mol^{-0.3}.(m_{elec}^2)^{-6}.(m^3)^{0.2}.s^{-1}$.

Section SM.7: Model resolution[1]

I. Initialization

- define all the partial reactional orders, $\alpha_{E\chi}, \beta_{E\chi}, \gamma_{E\chi}$, the kinetic constant, $k_{E\chi}$, the tortuosity, τ, and the porosity, ω, of the electrocatalytic layer domain Ω_{EC}, the diffusivity coefficient of urea, $D_{urea,w}$, and the cell volume, V;
- set the initial concentrations of soluble components in each subdomain: $[OH^-]_{\forall z,t=0}$ and $[CO(NH_2)_2]_{\forall z,t=0}$;
- set the geometrical surface, $S_{elec}^{geometric}$, and the rugosity of the electrode, Sdr. The Sdr parameter can be considered as the ratio between the area of the 'real' developed surface and the area of the 'projected' surface. In our case, the Sdr is measured by a 3D optical profiler (S-Neox, Sensofar®, Spain) and equal to 1.09%.
- calculate the real electrode surface S_{elec} according to Eq. (SM. 2);

$$S_{elec} = S_{elec}^{geometric} \times Sdr \qquad \text{(SM. 2)}$$

- calculate the kinetic apparent constant, k_{app};
- calculate the effective diffusivity coefficient of urea, $D_{urea,w}^{eff}$, into the Ω_{EC} domain;
- set the time $t = 0$ and the time step size $\tau_n = 1$ s;
- set the size and shape of computational sub-domains, Ω_B, Ω_F and Ω_{EC};
- initialize all the model fluxes to 0;
- calculate the dimensionless Biot number, Bi defined in Eq. (39).

II. Time stepping (pseudo-steady state)

do

Time step n at time t_n.

A. Dynamics of urea concentration in the electrocatalytic layer Ω_{EC} (steady state)

1. <u>Calculate dimensionless Hatta number</u>

   The Hatta number, defined as Eq. (SM. 3), allows to describe the competition, in the Ω_{EC} domain, between the chemical kinetics and the effective diffusion inside the porous solid. Depending on this number, either a chemical or diffusional regime takes place.

$$Ha = \sqrt{\frac{k_{app} \times \mu^2}{D_{urea,w}^{eff} \times [CO(NH_2)_2]^{0.7}}} \qquad \text{(SM. 3)}$$

2. <u>Solve mass balance:</u>

- Solve for urea concentration $[CO(NH_2)_2]_{\delta \le z \le \delta+\mu,\ t_n+\tau_n}$, the ODE system:

$$\frac{\partial^2[CO(NH_2)_2]}{\partial x^2} - Ha^2 \times [CO(NH_2)_2]^{0.3} = 0 \qquad \text{(SM. 4)}$$

from t_n to $t_n + \tau_n$.

A shooting method for boundary value problems of ODE system was used for stable and accurate integration between t_n and $t_n + \tau_n$. The method consisted in testing

[1] The presentation of the model resolution is inspired from the work of Picioreanu C., Head I.M., Katuri K. P., van Loosdrecht M. K., Scott K., A computational model for biofilm-based microbial fuel cells, *Water Research*. **2007**. doi: 10.1016/j.watres.2007.04.009

different fluxes in $z = \delta$ so as to minimize a target function defined in $z = \delta + \mu$ as a Neumann condition ($\frac{\partial[CO(NH_2)_2]}{\partial z}\Big|_{z=\Lambda_E} = 0$).

B. Dynamics of urea concentration in the liquid film layer Ω_F (steady state)

1. <u>Scaling the diffusion flux by the respective mass transport characteristics to the studied area:</u>

$$Biot \times \frac{\partial[CO(NH_2)_2]}{\partial z}\Big|_{z=\Lambda_{FEC}}^{\Omega_F} = \frac{\partial[CO(NH_2)_2]}{\partial z}\Big|_{z=\Lambda_{FEC}}^{\Omega_{EC}} \quad \text{(SM. 5)}$$

2. <u>Solve mass balance:</u>

- Solve for urea concentration $[CO(NH_2)_2]_{0\leq z\leq\delta,\ t_n+\tau_n}$

$$\frac{\partial^2[CO(NH_2)_2]}{\partial x^2} = 0 \quad \text{(SM. 6)}$$

C. Dynamics of urea concentration in the bulk Ω_B (transient state)

1. <u>Solve mass balance:</u>

- Solve for urea concentration $[CO(NH_2)_2]_{z\leq 0,\ t_n+\tau_n}$

$$V^{bulk} \times \frac{\partial[CO(NH_2)_2]_{z\leq 0}}{\partial t} + D_{urea,w} \times S_{electrode} \times \frac{\partial[CO(NH_2)_2]}{\partial z}\Big|_{z=\Lambda_{BF}}^{\Omega_F} = 0 \quad \text{(SM. 7)}$$

- Solve for urea concentration $[CO(NH_2)_2]_{z=\delta,\ t_n+\tau_n}$

$$[CO(NH_2)_2]_{z=\delta} = [CO(NH_2)_2]_{z=0} + \delta \times \frac{\partial[CO(NH_2)_2]}{\partial z}\Big|_{z=\Lambda_{BF}}^{\Omega_F} \quad \text{(SM. 8)}$$

Section SM.8: Data Availability

Table 1 Data produced by the experiments to obtain Figure 1

Entry	Figure 1-a				
	#1	#2	#3	#4	#5
$[CO(NH_2)_2]$ $[mmol.L^{-1}]$	20	30	50	200	250
$[OH^-]$ $[mmol.L^{-1}]$	5				
Purity of nickel(III) powder	79%				
$r_0^{\chi} \times 10^6$ $[mol.L^{-1}.(g_{cat}.s)^{-1}]$	3.9	5.5	5.9	7.9	6.4

Entry	Figure 1-b					
	#1	#2	#3	#4	#5	#6
$[CO(NH_2)_2]$ $[mmol.L^{-1}]$	10					
$[OH^-]$ $[mmol.L^{-1}]$	5	10	20	30	40	50
Purity of nickel(III) powder	79%					
$r_0^{\chi} \times 10^6$ $[mol.L^{-1}.(g_{cat}.s)^{-1}]$	20.8	23.3	44.6	46.3	58.5	46.4
$[CO(NH_2)_2]$ $[mmol.L^{-1}]$	50					
$[OH^-]$ $[mmol.L^{-1}]$	5	10	20	30	40	50
Purity of nickel(III) powder	79%					
$r_0^{\chi} \times 10^6$ $[mol.L^{-1}.(g_{cat}.s)^{-1}]$	5.9	9.7	12.2	15.3	16.1	13.2
$[CO(NH_2)_2]$ $[mmol.L^{-1}]$	100					
$[OH^-]$ $[mmol.L^{-1}]$	5	10	20	40	50	
Purity of nickel(III) powder	79%					
r_0^{χ} $[mol.L^{-1}.(g_{cat}.s)^{-1}]$	9.4	13.9	33.4	41.5	61.7	
$[CO(NH_2)_2]$ $[mmol.L^{-1}]$	150					
$[OH^-]$ $[mmol.L^{-1}]$	5	10	20	30	40	50
Purity of nickel(III) powder	79%					
r_0^{χ} $[mol.L^{-1}.(g_{cat}.s)^{-1}]$	20.9	33.2	45.1	69.48	75.0	79.5
$[CO(NH_2)_2]$ $[mmol.L^{-1}]$	300					
$[OH^-]$ $[mmol.L^{-1}]$	5	10	20	30	40	50
Purity of nickel(III) powder	79%					
r_0^{χ} $[mol.L^{-1}.(g_{cat}.s)^{-1}]$	2.7	13.1	16.1	18.9	21.5	20.1

Entry	Figure 1-c				
	#1	#2	#3	#4	#5
β_{χ} $[-]$	0.5	0.4	0.8	0.6	0.8

Entry	Figure 1-d				
	#1	#2	#3	#4	#5
$k'_{app} \times 10^2$ $[mol^{(1-\beta_{\chi})}.(m^3)^{(\beta_{\chi}-1)}.(g_{cat}.s)^{-1}]$	0.9	0.4	0.3	0.8	0.6

Table 2 Data produced by the experiments to obtain Figure 3

Entry	Figure 3-a					
	#1	#2	#3	#4	#5	#6
$[CO(NH_2)_2]$ $[mmol.\,L^{-1}]$	10	50	75	100	200	300
$[OH^-]$ $[mol.\,L^{-1}]$	1					
$S_{electrode}$ $[mm^2]$	3.14					
ν_{scan} $[mV.\,s^{-1}]$	0.12					
ω_{RDE} [RPM]	1000					
j_{lim} $[A.\,m^{-2}]$	21.7	36.3	38.9	45.0	57.6	65.4

Entry	Figure 3-b				
	#1	#2	#3	#4	#5
$[CO(NH_2)_2]$ $[mol.\,L^{-1}]$	0.3				
$[OH^-]$ $[mol.\,L^{-1}]$	0.1	0.25	0.5	1	1.5
$S_{electrode}$ $[mm^2]$	3.14				
ν_{scan} $[mV.\,s^{-1}]$	0.12				
ω_{RDE} [RPM]	1000				
j_{lim} $[A.\,m^{-2}]$	11.1	39.1	59.3	75.8	143.8

Entry	Figure 3-c			
	#1	#2	#3	#4
$[CO(NH_2)_2]$ $[mol.\,L^{-1}]$	0.3			
$[OH^-]$ $[mol.\,L^{-1}]$	1			
$S_{electrode}$ $[mm^2]$	8.7	9.2	10.4	15.4
ν_{scan} $[mV.\,s^{-1}]$	0.12			
$\omega_{magnetic\ stirrer\ bar}$ [RPM]	1000			
I_{lim} [A]	9.9E-5	3.3E-4	2.3E-4	1.7E-3